PHYSICAL REVIEW C **75**, 014905 (2007)

Strangeness chemical equilibration in a quark-gluon plasma

Jean Letessier
Laboratoire de Physique Théorique et Hautes Energies, Université Paris 7, 2 place Jussieu, F-75251 Cedex 05, France

Johann Rafelski
Department of Physics, University of Arizona, Tucson, Arizona 85721, USA
(Received 22 February 2006; published 19 January 2007)

We study, in the dynamically evolving quark-gluon plasma (QGP) fireball formed in relativistic heavy ion collisions at the BNL Relativistic Heavy Ion Collider (RHIC) and CERN Large Hadron Collider (LHC), the growth of strangeness yield toward and beyond the chemical equilibrium. We account for the contribution of the direct strangeness production and evaluate the thermal-QCD strangeness production mechanisms. The specific yield of strangeness per entropy, s/S, is the primary target variable. We explore the effect of collision impact parameter, i.e., fireball size, on kinetic strangeness chemical equilibration in QGP. Insights gained in studying the RHIC data with regard to the dynamics of the fireball are applied to the study of strangeness production at the LHC. We use these results and consider the strange hadron relative particle yields at RHIC and LHC in a systematic fashion. We consider both the dependence on s/S and the direct dependence on the participant number.

DOI: 10.1103/PhysRevC.75.014905 PACS number(s): 25.75.Nq, 24.10.Pa, 12.38.Mh

I. INTRODUCTION

Conversion of kinetic collision energy into high multiplicity of newly made hadronic particles is one of the most notable features of reactions observed at the Relativistic Heavy Ion Collider (RHIC) at the Brookhaven National Laboratory (BNL) [1]. In this process, aside from the light u and d quark pairs present in all matter surrounding us, the strange flavor quark pairs $s, \bar{s}$ are produced copiously (in general, in what follows, the particle symbol will refer to the corresponding particle yield, either total or per unit of rapidity, as appropriate). The final s yield depends on the initial reactions and on the history of the fireball, and thus, it also depends on the nature and properties of the phase of matter formed. On the time scale of hadronic interactions, strangeness flavor is conserved, and prior to any weak interaction decays, we have $\bar{s} = s$; when we refer to strangeness yield, production, etc., we always address the yield, production, etc., of strange quark pairs.

This study is addressing strangeness under the physical conditions achieved at RHIC at the highest attainable reaction energy today, $\sqrt{s_{\rm NN}} = 200$ GeV, and in the future at the CERN Large Hadron Collider (LHC). We are particularly interested in the sensitivity of strangeness production to the nature and properties of the matter formed in the heavy ion reactions. Theoretical studies have shown that strangeness is produced rapidly in collisions (fusion) of thermalized gluons [2,3], within the deconfined state, the quark-gluon plasma (QGP) formed in the central collisions of heavy nuclei. On the scale of the RHIC reaction time $\tau < 10$ fm, the hadron-based reactions were found to be too slow to allow copious strangeness production after thermalization of matter and are even more ineffective for producing multistrange hadrons [5].

On the other hand, strangeness can be produced fast in the QGP phase, as we shall see, achieving near chemical equilibrium in QGP phase formed at RHIC and even overshooting the chemical equilibrium at hadronization at the LHC. Thus, the situation is quite different when the deconfined QGP state breaks up in a fast hadronization process: the enhancement of strange hadrons and most specifically strange antibaryons, growing with valance strange quark content of hadrons produced is the predicted characteristic property of the deconfined QGP phase [6]. This happens because in the breakup of the strangeness rich deconfined state, i.e., hadronization, several strange quarks formed in prior, and independent, reactions can combine into a multistrange hadron.

Our main objective in this work is to quantify the mechanisms of kinetic strangeness production occurring in thermal gluon collision (fusion) processes during the expansion phase of the quark-gluon fireball. We explore the centrality dependence in a wide range between peripheral, and most central reactions, in which up to 90% of projectile and target nucleons participate. In this regard, this paper is a theoretical companion to the more phenomenological analysis of experimental RHIC data [7,8], and uses the insights gained in this analysis, in particular, regarding the dynamics of the QGP expansion. This is then applied to extrapolate our approach to the LHC energy domain, where our prior particle yield study was based on a parametric consideration of final state strangeness yield [9].

We also study in depth the centrality dependence of strangeness production in the RHIC-LHC energy range. As the centrality of the nuclear reaction and the number of participants A decreases, the number of thermal collisions gradually diminishes, and with it the strangeness enhancement effect also diminishes gradually, similar to that seen in the energy range of the BNL Alternating Gradient Synchrotron (AGS) and CERN Super Proton Synchrotron (SPS) [3,4]. This decrease drives in turn a gradual decrease in the centrality dependent production rate of multistrange hadrons. This behavior, which we discuss in detail here, is an important and characteristic phenomenological feature of the kinetic particle collision mechanism of strangeness production and enhancement.

Interestingly, in this regard, the kinetic mechanism of strangeness production differs from models such as the canonical enhancement model, which derives the strange hadron enhancement as a result of an always prevailing hadronic phase chemical equilibrium [10,11]. The volume dependence of the canonical phase space yields [12] and the smallness of the *N*-*N* reference systems produce the centrality enhancement effect [13]. However, canonical enhancement rises very rapidly considering the rather small collision systems, and with decreasing energy [14].

The understanding of strangeness production during the expansion phase of the quark-gluon fireball allows us to study in depth the reaction mechanisms which are determining the final state yield of strangeness. In this way, we learn how deeply into the history of QGP expansion this observable allows us to look. Collective matter flow features observed at RHIC suggest that thermalization of parton matter occurred very fast, i.e., the entropy S has been produced in a not yet fully understood fast process of parton thermalization, prior to the production of the strangeness pair yield s. We formulate the kinetic equations allowing us to address, in some detail, the growth in specific strangeness per (fixed) entropy s/S in the thermal QGP processes in both a longitudinally and transversely expanding QGP fireball.

The time evolution of s/S was considered for the first time early in the development of the QGP physics [15]. However, the model of dense matter evolution and the range of statistical parameters considered at the time are not appropriate for the RHIC and LHC physics environments. Moreover, we recompute here the rate of strangeness production using the best current values of QCD parameters, the coupling constant α_s, and the strange quark mass m_s. These parameters alter decisively the values of s/S in chemical equilibrium, and thus the dynamical time scale of the approach to chemical equilibrium. To compute the evolution in time of s/S, we must also evaluate how near to chemical equilibrium is the strangeness in QGP; this nearness is characterized by the parameter γ_s, which is roughly the ratio of the prevailing strangeness density to the chemical equilibrium density at the prevailing temperature.

Setting up the production of strangeness, we assume here that it follows in time the chemical equilibration of the light $q = u, d$ quarks and g gluons [16], which are believed to occur at 1 fm scale. These effectively massless particles can be produced by entirely soft processes which are intrinsically nonperturbative [17]. Their chemical equilibration can be further driven by multiparticle collisions [18,19]. Considering these studies, we assume here relatively short relaxation times for q, g, we cannot compute these using the same perturbative method as will be developed here to evaluate strangeness yield equilibration. It is the finite strangeness mass combined with the measured strength of the running QCD coupling constant α_s which allows us the use of perturbative formalism in the study of strangeness production [20] with some minimal confidence.

The chemical relaxation times for the strangeness approach to chemical equilibrium, in an expanding QGP, has been considered several times before [3,21–26]. The study of QGP strangeness chemical equilibration must not be confused with the phenomenological investigation of chemical equilibrium in the final state hadron abundance. Because hadron phase space is generally smaller, chemical equilibrium and indeed excess over equilibrium is much more easy to attain, and there is some continuing discussion of this question [27–29].

We offer in our work a comprehensive exploration of how the impact parameter dependence, and consideration of energy dependence, influences chemical equilibration in QGP. We evolve in time not the strangeness itself but the specific strangeness per entropy s/S. In this way, we can identify more clearly the production processes of strangeness, since entropy is produced earlier on, and is (nearly) conserved during the time period of thermal strangeness production.

Importantly, s/S is an experimental observable, practically preserved in the fast hadronization process. Thus, we can connect the final state of the QGP evolution directly to experimental soft hadron yield experimental results. We find that much of the variability about the initial conditions, such as dependence on initial temperature, cancels in the final result. This specific observable will be shown to yield nearly model independent insights about thermal strangeness production in QGP.

In Sec. II, we begin with a brief discussion of general features relevant to all considerations presented. In Sec. II D, we formulate the kinetic equations describing the growth in specific strangeness per entropy s/S and show that, at RHIC, the observed specific per entropy strangeness yield suggests that the "direct" and "thermal" processes are of comparable strength in most central reactions. We discuss the magnitude and importance of QCD parameters in Sec. II E. In order to integrate as a function of reaction time the strangeness yield equations, we develop a simple collective expansion model of the plasma phase in Sec. II F.

In Sec. III, we study the thermal strangeness production processes. We then obtain reference yields for two different expansion geometries at RHIC in Sec. III A. We extrapolate this to the LHC environment in subsection III B. We explore in Sec. III C how deeply into the early history of the hot, dense fireball the strangeness signature of thermal QGP is allowing us to look, i.e., the dependence on initial conditions; importantly, we find that the selection of the initial value of s/S related to direct production of strangeness has only a minor impact on the final results regarding strangeness yield. We then explore the influence of fundamental uncertainties, such as the present day limited knowledge about the strange quark mass and the QCD thermal effects on the freezing of the strange quark degrees of freedom, in Sec. III D.

In Sec. IV, we connect the results we obtained to the experimental particle yields. In Sec. IV A, we consider the relationship between hadron multiplicity and entropy yield, and obtain the strange hadron yield as function of s/S. This allows an assessment of how strangeness yields, at RHIC and LHC, influence physical observables. In particular, we discuss how K^{+/π^+} changes between these two experimental environments. Then, we discuss, in Sec. IV B, for the two most often used statistical hadronization models [sudden hadronization and chemical equilibrium hadronic gas (HG) hadronization] the production of strange hadrons as a function of participant number A, keeping the hadronization condition

independent of A. In Sec. IV C, we apply the insights gained in the study of thermal strangeness production to evaluate thermal charm production at the RHIC and LHC environments.

II. REMARKS ABOUT STRANGENESS PRODUCTION AND DENSITY

A. Parton equilibration and strangeness production

The total final state hadron multiplicity is a measure of the entropy S produced prior to thermal production of strangeness s in QGP: once a quasithermal exponential energy distribution of partons has been formed, the entropy production has been completed. Further evolution of the dense deconfined fireball is nearly entropy conserving, even though it is strangeness flavor producing: fusion of gluons, or light quark pair annihilation into strangeness, is a nearly entropy conserving process [30]. We note that in reactions between two thermal particles into a strangeness pair, the energy content of each initial state parton is transferred to the two reaction products, so thermal partons produce the thermal shape of the strangeness spectrum.

The entropy produced in RHIC reactions has been evaluated in recent studies of hadron multiplicities. In Au-Au reactions, at $\sqrt{s_{NN}} = 200$ GeV, one sees $S \simeq 35000$. Furthermore, at central rapidity, the yield of entropy is $dS/dy \simeq 5000$. In the benchmark results we present for LHC, we will assume that the the central rapidity entropy yield is about 4 times greater than that for RHIC.

The temporal evolution of the QGP fireball ends when the temperature has decreased to the QGP hadronization value. In the breakup of the QGP, the hadron yields are established, and it is rather difficult to alter these yields appreciably in the ensuing rather short-lived evolution lasting not more than 1.5 fm/c . Thus, the hadronization volume, with the normalizing factor dV/dy, provides the normalization of hadron particle yields per unit of rapidity. The final value of $dV(\tau_f)/dy$ is the result of the analysis of hadron particle yields, and our model of the time dependence of $dV(\tau)/dy$ will be constrained by the magnitude of dV_f/dy obtained in Ref. [7].

There are two separate stages of strangeness (charm) production, corresponding to the two practically distinct periods of the fireball evolution: (a) direct production, which creates a background yield corresponding to what might be obtained in a superposition model of independent nucleon-nucleon (N-N) reactions, and (b) strangeness production in collisions between thermally equilibrated QGP constituents.

For (b) to be relevant, prior formation of a thermal, deconfined QGP phase is required. Without process (b), the yield of strangeness should not be enhanced in A-A collisions as compared to scaled N-N reactions. We will not discuss in detail mechanism (a) of direct particle production here, because our interest is restricted to (approximate) initial yields, which are the baseline for the thermal mechanisms acting in the QGP and define the strength of any enhancement.

We note for the record that strangeness initial production, like other relatively soft parton production processes, is believed to be due to a color string breaking mechanism [31], and the PYTHIA6 model of soft hadron production presumes that the relative strength of $u : d : s$ production is $1 : 1 : 0.3$. The (initial) charm production is due to high-energy parton collisions [32].

Our study of thermal strange particle production processes is based on kinetic theory of particle collisions. There is considerable uncertainty about the initial momentum distributions of soft partons present in the initial state. However, two recent theoretical studies argue that there is rapid thermalization. The nonlinear gluon production processes lead to the gluon momentum distribution equilibration [19]. Axial asymmetry of the initial state causes collective instabilities which further accelerate thermalization of partons [33].

In this context, it is important to advance one result of our study, namely, that there is little sensitivity to the initial thermal condition: a wide range of reasonable initial temperatures lead to very similar strangeness production results, as long as the entropy content is preserved. In order to understand this, consider a decrease in initial temperature. This requires, at fixed entropy, an increase in initial volume, and this, then, is associated with an increased lifespan of the fireball in the high-temperature strangeness producing domain. These two effects combine to compensate for the reduced strangeness production rate per unit of time and volume that is associated with reduced ambient temperature.

We believe that this mechanism also implies that the precise form of the momentum spectrum of the initial state partons is of minor practical relevance to the evaluation of strangeness production, and we do not study this. Therefore, without loss of generality, we can assume that the parton distributions we use in the kinetic strangeness formation process have a thermal shape, and the ambient temperature is determined considering the (lattice fitted) equation-of-state relation of initial temperature and entropy density [34] for a given geometric initial volume.

We already remarked that the production of strangeness in a cascade of N-N reactions (without deconfinement) is not able to add significantly to the initial strangeness yield considering the short lifespan of the fireball. Thus, this alternative will not be further considered in this work. Similarly, any additional strangeness produced in the rapid hadronization of QGP into hadrons must be negligible compared to the thermal production process which occurs at higher particle density (temperature) and during a considerably longer lifespan.

B. Approach to chemical yield equilibrium

It has been shown, considering the entropy maximization principle, that the approach of particle densities to chemical equilibrium density ρ_i^∞ can be characterized by the statistical parameter γ_i [35], which varies with the local proper time τ during the collision. For example, for gluons,

$$\rho_g(\tau) \equiv \int d^3p \frac{\gamma_g(\tau) e^{-E/T}}{1 - \gamma_g(\tau) e^{-E/T}}, \quad E = \sqrt{m^2 + p^2}. \quad (1)$$

Generally, the Lagrangian mass of gluons is zero. However, one may be tempted to think that thermal mass $m(T)$ could decisively change the results, suppressing the collisional strangeness production. However, one finds that instead the process of gluon decay becomes relevant, and, if at all, there

is a net rate increase of strangeness production [36]. One could argue that the scheme to study the kinetic process of strangeness chemical equilibration using thermal mass amounts to a different resummation of reaction processes. In this work, we will consider the evolution of $\gamma_s^{\rm QGP}(\tau)$ based on Lagrangian masses, allowing for $\gamma_g^{\rm QGP}(\tau)$ and $\gamma_q^{\rm QGP}(\tau)$.

For strange quarks, we will keep only the Boltzmann term [ignoring the denominator in Eq. (1) above], and thus,

$$\rho_s(\tau) \equiv \gamma_s^{\rm QGP}(\tau)\rho_s^{\infty} = \gamma_s^{\rm QGP}\frac{g_s}{2\pi^2}z^2K_2(z), \quad z = \frac{m_s}{T}. \quad (2)$$

Here, g_s is the strange quark degeneracy, and K_2 is a Bessel function. Since we will employ strangeness occupancy in the hadron phase, γ_s^h, we have included the superscript QGP. We will henceforth drop this superscript, and occupancy parameters without the superscript will, in general, refer to the QGP phase, while the hadronic gas phase variable, when these are expected to differ from QGP, will have a superscript h.

Our target variable is the final QGP state specific yield of strangeness per entropy, s/S, and the related phase space occupancy γ_s. Both these variables have an important physical relevance: s/S determines the final yield of strange hadrons compared to all hadrons, and its value implies some particular yield of reference yields, such as, e.g., K^+/π^+. Whereas γ_s, which characterizes the approach to chemical equilibrium, measures the strangeness yield in terms of the chemical equilibrium yield. The strangeness phase spaces of QGP and HG phases are different. Strangeness in QGP is much denser than in the HG phase, considering the range of strange quark masses, $0.080 < m_s(\mu\,2\,{\rm GeV}) < 0.125\,{\rm GeV}$. Therefore, (near) chemical strangeness equilibrium in the QGP phase, $\gamma_s \simeq 1$, implies a significantly oversaturated hadron phase space abundance $\gamma_s^h > 1$ after hadronization. γ_s^h is directly controlling the relative yields of hadrons with different $s + \bar{s}$ valance quark content and is thus observable.

C. Role of initial conditions

We do not understand well the conditions in the QGP phase at times as early as $\tau_0 = 0.25$ fm for RHIC and $\tau_0 = 0.1$ fm for LHC, when we presume that the thermal momentum distribution is practically established. Thus, we must make a number of assumptions and check if these impact our results. The following relevant parameters could govern the strangeness production:

(i) $\gamma_g(\tau)$ and, in particular, the initial value at τ_0;
(ii) τ_0, the time at which we assume thermal momentum of partons is reached;
(iii) $s/S|_{\tau_0}$, the initial strangeness yield originating in direct parton collisions;
(iv) $R_\perp$, the transverse radius dimension at initial time, related to the collision geometry;
(v) $v_\perp(\tau)$, the transverse expansion velocity and, in particular, its maximum value at hadronization; and
(vi) τ_g and τ_q, the relaxation time constants of gluon and quark fugacities (considering that quarks are less relevant compared to gluons with regard to strangeness production, we will assume $\tau_q = 1.5\ \tau_g$ throughout this work).

We explore, here, a characteristic gluon thermalization time $0.1 < \tau_0 < 1.5$ fm/c, with the longest value applicable to most peripheral RHIC Au-Au reactions at $\sqrt{s_{NN}} = 200$ GeV, and the shortest period assumed for the future LHC central collisions. Knowing the exact dynamics of thermalization and how long it takes will be, as we shall see, rather unimportant for the final insights we obtain.

All initial state parameters are constrained in their value by collision geometry, by final state particle yields observed at RHIC, or/and by particle correlations. For example, the final yields of strangeness ds/dy and entropy dS/dy and thus s/S are known from an analysis of particle production: as a function of centrality at RHIC [7], and as a function of reaction energy from the top AGS and SPS to the top RHIC energies [37].

We will use these results in two ways. We compute, following the temporal evolution, the final state s/S ratio which we expect to converge at RHIC to $s/S \simeq 0.033$. We need to specify the initial value at time τ_0 for this variable, and this value is chosen to be compatible with the peripheral reactions. The entropy yield dS/dy, which we assume is conserved during the evolution of QGP, determines, for a known initial volume $dV(\tau = \tau_0)/dy$, the entropy density $\sigma = (dS/dy)/(dV/dy)$. We then can obtain, from standard properties of QGP fitted to the lattice results, the initial temperature $T_0/T_c \simeq 3$–4. This temperature decreases as volume expands with τ given that the entropy is preserved.

We will show that the two physical observables we address, s/S and γ_s, are largely independent of the model-dependent details of the initial conditions. Said differently, our important finding is that the two global strangeness observables s/S and γ_s appear to penetrate back only to about 2 fm/c after the reaction has begun and do not probe earlier conditions in the QGP phase. The physical reason for this is, of course, that once chemical equilibrium is approached, one loses much of the event memory with regard to intensive physical observables. We will further see that in cases we studied that did not quite reach chemical equilibrium in the QGP phase, this is also true, i.e., there is little sensitivity to what exactly happened to light quarks and gluons in the first 2 fm/s.

The reason for this is that there is a strong correlation between volume, temperature, and degree of QGP (gluon and light quark) chemical equilibration, as we already discussed above. Repeating the argument differently, we can say that when fewer gluons at fixed entropy are in a given volume, temperature has to be larger. Thus, any decrease in the production of strangeness in gluon fusion due to absence of gluons is compensated by the greater specific rate per colliding pair due to greater ambient temperature. Hence, also when we do not quite reach chemical equilibrium in QGP, be it due to large impact parameter or low reaction energy (chemical nonequilibrium at lower energies is not explored in this paper), there is little if any dependence of thermal yield on initial conditions, and the results we arrive at regarding near chemical equilibration are extraordinarily robust.

However, the thermal strangeness production does depend on the degree of initial state strangeness equilibration, simply

because if the initial yields were chemically equilibrated to start with, there would be as much production as annihilation of strangeness and any temporal evolution is driven by the time dependence of the evolution dynamics. We will take as a measure of the pre-QGP thermal phase strangeness production the specific per hadron multiplicity yield of strangeness observed in most peripheral RHIC reactions. This is typically $s/S \simeq 0.016$ at $\tau = \tau_0$. This choice allows us to reproduce the observed value $s/S = 0.019$ attained in most peripheral nuclear reactions at RHIC [7], with a participant number about $\langle A\rangle = 6.3$. Clearly, with $s/S \to 0.033$ in most central collisions, the implication of this choice is that the thermal process enhances total specific yield by a factor of 1.9 ± 0.3. As centrality and/or reaction energy decreases, there is a gradual decrease of this enhancement, and as the energy is increased (LHC), this enhancement rises somewhat.

D. Strangeness production in thermal collisions

We follow the established methods of evaluating thermal strangeness production [38], expanding our earlier more schematic model [24]. However, considerable simplification arises since we focus attention on the specific yield of strangeness per entropy.

In the local (comoving) frame of reference, the rate of change of strangeness is due to production and annihilation reactions only, that is,

$$\frac{1}{V}\frac{ds}{d\tau} = \frac{1}{V}\frac{d\bar{s}}{d\tau} = \frac{1}{2}\rho_g^2(t)\langle\sigma v\rangle_T^{gg\to s\bar{s}} + \rho_q(t)\rho_{\bar{q}}(t)\langle\sigma\rangle_T^{q\bar{q}\to s\bar{s}} - \rho_s(t)\rho_{\bar{s}}(t)\langle\sigma v\rangle_T^{s\bar{s}\to gg,q\bar{q}}. \tag{3}$$

The thermally average cross sections are

$$\langle\sigma v_{\rm rel}\rangle_T \equiv \frac{\int d^3p_1 \int d^3p_2 \sigma_{12} v_{12} f(\vec{p}_1, T) f(\vec{p}_2, T)}{\int d^3p_1 \int d^3p_2 f(\vec{p}_1, T) f(\vec{p}_2, T)}. \tag{4}$$

$f(\vec{p}_i, T)$ are the relativistic Boltzmann/Jüttner distributions of two colliding particles $i = 1, 2$ of momentum p_i, characterized by local statistical parameters.

A convenient way to address the dilution phenomena acting on the density of strangeness $\rho_s \equiv s/V$ due to rapid expansion of the QGP phase, Eq. (3), is to consider the proper time evolution of the specific strangeness per entropy yield:

$$\frac{d}{d\tau}\frac{s}{S} = \frac{V}{S}\frac{1}{V}\frac{ds}{d\tau}. \tag{5}$$

The entropy S in a volume element is unchanged, as volume grows and temperature drops,

$$S = V\frac{4\pi^2}{90}g(T)T^3 = \text{Const.}, \tag{6}$$

where we consider the quark and gluon degrees of freedom along with their QCD corrections:

$$g = 2_s 8_c\left(1 - \frac{15\alpha_s(T)}{4\pi} + \cdots\right) + \frac{7}{4}2_s 3_c n_f\left(1 - \frac{50\alpha_s(T)}{21\pi} + \cdots\right). \tag{7}$$

We use as the number of quark flavors $n_f \simeq 2 + \gamma_s 0.5 z^2 K_2(z)$, where $z = m_s/T$. The terms proportional to chemical potentials are not shown in the expression for entropy, since $\mu/\pi T \ll 1$ at RHIC and LHC.

We have used, here, the lowest order QCD corrections to the effective degeneracies, since these describe well the properties of QGP phase obtained on the lattice [34], when the value of $\alpha_s(T)$ used is as described below, see Eq. (12). The agreement one sees for thermodynamic variables, such as E, P, S, with the lattice results is very remarkable, including the temperature range near to the phase boundary. Thus, the use of constraint Eq. (6) to evaluate the time dependence of temperature, considering also that the third root of entropy is considered, should yield precise enough results. We note, in passing, that we used as specified in Ref. [34] the additional terms $\mathcal{A}$ in entropy, arising from differentiation of the implicit temperature dependence of g, Eq. (7) entering the partition function.

In order to use the detailed balance which relates production and annihilation reactions, it is convenient to introduce the invariant rate per unit time and volume, $A^{12\to 34}$, by incorporating the equilibrium densities into the thermally averaged cross sections:

$$A^{12\to 34} \equiv \frac{1}{1+\delta_{1,2}}\gamma_1\gamma_2\rho_1^\infty\rho_2^\infty\langle\sigma_s v_{12}\rangle_T^{12\to 34}. \tag{8}$$

$\delta_{1,2} = 1$ for the reacting particles that are identical bosons; otherwise, $\delta_{1,2} = 0$. Note also that the evolution for s and $\bar{s}$ in proper time of the comoving volume element is identical as both change in pairs.

We find that the temporal evolution of s/S, in an expanding plasma, is governed by

$$\frac{d}{d\tau}\frac{s}{S} = \frac{A^{gg\to s\bar{s}}}{(S/V)}\left[\gamma_g^2(\tau) - \gamma_s^2(\tau)\right] + \frac{A^{q\bar{q}\to s\bar{s}}}{(S/V)}\left[\gamma_q^2(\tau) - \gamma_s^2(\tau)\right]. \tag{9}$$

When all $\gamma_i \to 1$, the Boltzmann collision term vanishes, and equilibrium has been reached. The value arrived at for the observable s/S depends on the history of how the system evolves and, eventually, reaches equilibrium.

To solve Eq. (9), we need a relation between s/S and γ_s. This is obtained by combining strangeness density Eq. (2) and entropy Eq. (6):

$$\frac{s}{S} = \gamma_s\frac{g_s}{g}\frac{90}{8\pi^4}z^2K_2(z), \quad z = m_s/T. \tag{10}$$

In the initial period, gluons and quarks have not reached chemical equilibrium; thus, the actual numerical integrals of Bose and Fermi distributions of the type in Eq. (1), dependent on the values $\gamma_{q,g}$, are employed instead, which modifies the result seen in Eq. (10).

The degeneracies we have considered in Eq. (6) for the entropy did include the effect of interactions, and thus we have to allow for the interaction effect in the strange quark degeneracy as well:

$$g_s = 2_s 3_c\left(1 - \frac{k\alpha_s(T)}{\pi} + \cdots\right). \tag{11}$$

The value of $k = 2$ applies to massless strange quarks. At $T = 0$ (or, said differently, for $m \gg T$), the early study of quark matter self-energy suggests that $k \to 0$ [39]. We will present, in Fig. 6 below, results for varying values of k, and the reference value we use in our other studies is $k = 1$. We believe that this approach allows us to explore the general behavior of the interactions effect on the strangeness density, a more detailed study is not possible today.

E. QCD parameters

We evaluate $A^{gg\to s\bar{s}}$ and $A^{q\bar{q}\to s\bar{s}}$ employing the available strength of the QCD coupling and range of accepted strange quark masses. In our evaluation of strangeness production, in order to account for higher order effects in quark and gluon fusion reactions, we introduce a multiplicative $K = 1.7$ factor. The known properties of QCD strongly constrain our results [3]. However, it turns out that the range of strange quark masses remains sufficiently wide to impact the results, and we discuss this further in Sec. IV A, see Fig. 7 below. We employ when not otherwise stated the central value from a recent PDG evaluation, $m_s(\mu = 2\,\text{GeV}) = 0.10\,\text{GeV}$ which remains uncertain at the level of 25% at least. In fact, since our results were obtained, a more recent Particle Data Group (PDG) study recommends a 10% smaller central value of m_s.

We compute rate of reactions employing a running strange quark mass working in two loops and using as the energy scale the c.m. reaction energy $\mu \simeq \sqrt{s}$. Since the running of mass involves a multiplicative factor, the uncertainty in the mass value discussed above is the same for all values of μ. Some simplification is further achieved by taking at temperature T the value $\mu \simeq 2\pi T$ which is the preferred value of the thermal field theory and agrees with the value of the reaction energy. This means that we use $m_s(T) = m_s(\mu = 2\pi T)$ with $m_s(T = 318\,\text{MeV}) = 0.1$ GeV. The actual temperature $T(t)$ and thus time-dependent values of the strange (and charm) quark mass will always be shown in the top panel of figures describing the evolution of the properties of the system considered.

The strength of the QCD coupling constant, is today much better understood. We use as a reference value $\alpha_s(\mu = m_{Z^0}) = 0.118$, and we evolve the value to the applicable energy domain μ by using two loops. Our ability to use perturbative methods of QCD to describe strangeness production, a relatively soft process, derives from two circumstances:

(i) The reaction processes which change yield of strangeness can compete with the fast $v_\perp > 0.5c$ expansion of QGP only for $T > 220$ MeV; for lower temperatures, the strange quark yields effectively do not change (strange quark chemical freeze-out temperature in QGP). Using the relation $\mu = 2\pi T$, this implies that all strangeness yield evolution occurs for $\mu > 1.4$ GeV.
(ii) Because of the magnitude $\alpha_s(\mu = m_{Z^0}) = 0.118$, one can quite well run α_s to the scale of interest, $\mu > 1.2$ GeV.

As we see in Fig. 1, this means that the strength of the interaction remains $\alpha_s < 0.5$. We also note that had the strength of $\alpha_s(\mu = m_{Z^0})$ been 15% greater, strangeness production could not have been studied in the perturbative approach.

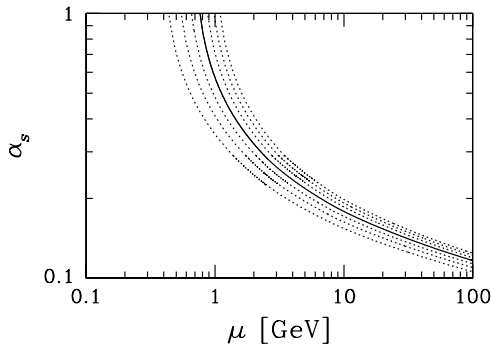

FIG. 1. Running QCD coupling constant $\alpha_s(\mu)$ fixed to $\alpha_s(\mu = m_{Z^0}) = 0.118$ (solid line) and several alternative strength scenarios excluded today by experimental measurement (dashed lines).

We next express $\alpha_s(\mu)$ (solid line in Fig. 1) as function of temperature by the conditions $\alpha_s(T) = \alpha_s(\mu = 2\pi T)$. This leads to the expression (see also Sec. 14 in [38])

$$\alpha_s(T) \simeq \frac{\alpha_s(T_c)}{1 + C\ln(T/T_c)}, \quad T < 6\,T_c, \tag{12}$$

with $C = 0.760 \pm 0.002$, and $\alpha_s(T_c) = 0.50 \pm 0.04$ at $T_c = 0.16$ GeV. We stress that Eq. (12) is a parametrization corresponding to the result shown in Fig. 1. Only one logarithm needs to be used to describe the two loop running with sufficient precision, since the range we consider is rather limited, $0.9\,T_c < T < 6\,T_c$.

F. Expansion and cooling of QGP

We separate, in our work, the issue of strangeness production from the even more complex and less understood questions about the time evolution of the QGP. We assume that there is some active volume at average temperature T in which the strangeness is "cooked." We derive the time dependence of local temperature from the hypothesis of a conserved entropy content and a reasonable model describing the volume evolution in time. This is arrived at using a hydrodynamically inspired model.

The volume at hadronization is an implicit observable. All particle yields at hadronization are normalized with a volume factor. Thus, our expansion model must be realistic enough so that the hadronization conditions are in agreement with data, and that the impact parameter dependence is reproduced. In the geometrically inspired model, we consider, in the central rapidity domain,

$$\frac{dV}{dy} = A_\perp(\tau)\left.\frac{dz}{dy}\right|_{\tau=\text{Const.}}. \tag{13}$$

dV/dy is the normalization factor for the particle yields we are measuring in an interval around the central rapidity. The transverse expansion is described by the transverse size $A_\perp(\tau)$. We further need to associate with the domain of rapidity dy a geometric region at the source dz, from which particles emerge.

To accomplish this, we recall the space-time rapidity of the scaling Bjørken hydrodynamic solution:

$$y = \frac{1}{2}\ln\frac{t+z}{t-z}. \tag{14}$$

We see that $y = 0$ corresponds to $z = 0$. In particular, if the transverse extent of the fireball is large, the Bjørken space-time rapidity relation prevails.

We need this relation not at a fixed laboratory time t but at some fixed proper time τ:

$$\tau = \sqrt{t^2 - z^2}. \tag{15}$$

We eliminate t in Eq. (14) using Eq. (15):

$$z = \tau \sinh y, \qquad \frac{dz}{dy} = \tau \cosh y. \tag{16}$$

$A_\perp$ is the transverse to scattering axes size of the evolving QGP. For nearly homogeneous expanding bulk matter, one can assume

$$A_\perp = \pi R_\perp^2(\tau). \tag{17}$$

However, if the matter is predominantly concentrated near a narrow domain of width d, we consider

$$\begin{aligned} A_\perp &= \pi\left[R_\perp^2(\tau) - \left(R_\perp^2(\tau) - d\right)^2\right], \\ &= 2\pi d\left[R_\perp(\tau) - \frac{d}{2}\right]. \end{aligned} \tag{18}$$

At central rapidity, we consider quantitatively the two evolution scenarios, denoted hence-forth as models V1 and V2. V1 will be the most simple bulk homogeneous expansion, while V2 simulates a transverse donut, corresponding to expansion with a cold hole of matter in the fireball (axial) center:

$$\text{V1}: \quad \frac{dV}{dy} = \pi R_\perp^2(\tau)\tau, \tag{19}$$

$$\text{V2}: \quad \frac{dV}{dy} = 2\pi d\left[R_\perp(\tau) - \frac{d}{2}\right]\tau, \tag{20}$$

with

$$R_\perp(\tau) = R_0 + \int v(\tau)d\tau. \tag{21}$$

Any model of transverse matter expansion dynamics $v(\tau)$ is constrained by the transverse mass shape of produced particle spectra; too large transverse velocities would produce too hard spectra. Accordingly, a hydro-inspired shape is assumed:

$$v(\tau) = v_{\max}\frac{2}{\pi}\arctan[4(\tau - \tau_0)/\tau_v]. \tag{22}$$

Values of $v_{\max}$ we consider are in the range of 0.5–0.8c, the relaxation time $\tau_c \simeq 0.5$ fm, and the onset of transverse expansion τ_0 was tried in the range 0.1–1 fm. None of these parameters matters for what follows as long as one does not employ aberrant values.

The initial size $R_\perp$ is assumed, in what follows, to be $R_\perp = 5$ fm for the 5% most central collisions. When we study centrality dependence, we will show results for a series of centralities decreasing the transverse dimensions $R_\perp$ and d by factor $f_R = 1.5$ in each step. We further scale the entropy value with $f_S = f_R^{2.2}$. This ensures that the dependence of entropy on the participant number $dS(A)/dy$ in the final state follows the relationship,

$$\frac{dS}{dy} \simeq 8(A^{1.1} - 1), \tag{23}$$

obtained from the impact parameter dependent fit to the RHIC impact parameter results [7].

An overview of the resulting volume dynamic behavior is given in Fig. 2; the top panel applies to RHIC with $\sqrt{s_{NN}} = 200$ GeV, the bottom panel presents a parallel study for LHC with the *assumed* four times greater entropy content. The solid lines are for transverse homogeneous volume (V1 model) expansion, and dashed lines correspond to a transverse region of thickness $d = 3.5$ fm (V2 model).

Three different centralities were considered with $R_\perp = 3$, 5 and 7 fm. For the second model of transverse expansion, the transverse size d is scaled with $R_\perp = 5$ fm. Thus, $d = 2.1$ fm for $R_\perp = 3$ fm, and $d = 4.9$ fm for $R_\perp = 7$ fm. Similarly, entropy content, assumed to be $dS/dy = 5000$ at RHIC and $dS/dy = 20000$ at LHC for $R_\perp = 5$ fm, is scaled to values $dS(R_\perp = 3\text{fm})/dy = 1300$ and $dS(R_\perp = 7\text{fm})/dy = 10500$, and correspondingly, four times greater values for LHC.

The temporal expansion of the volume is followed till $T = 140$ MeV is reached. In general, the maximum volume at LHC is thus four times greater than that at RHIC. The expansion time is correspondingly longer, with RHIC taking 6.5 fm to freeze-out for $R_\perp = 5$ fm; the LHC lifespan is 10 fm. The QGP lifespan increases by as much as 60% at LHC, when comparing it to the lifespan at RHIC, if the assumed initial

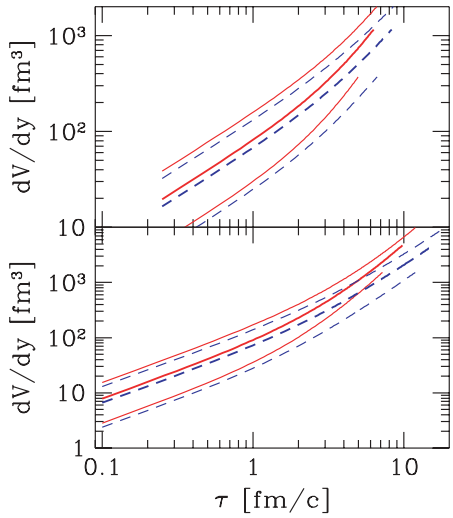

FIG. 2. (Color online) QGP volume related to central rapidity dV/dy as function of proper time τ. Top panel: RHIC with reference entropy content $dS/dy = 5000$ (central lines); bottom panel: LHC with four times greater entropy content $dS/dy = 20000$ (central lines). Three centralities are considered: middle thicker lines correspond to $R_\perp = 5$, and the upper and lower lines to $R_\perp = 7$ and, respectively, $R_\perp = 3$ fm/c. Solid lines are for V1 model with transverse homogeneity; dashed lines for V2 model of a transverse shell with widths (top to bottom) $d = 2.1$, 3.5, and 4.9 fm. Volume expansion is shown up to $T = 140$ MeV. See text for more details.

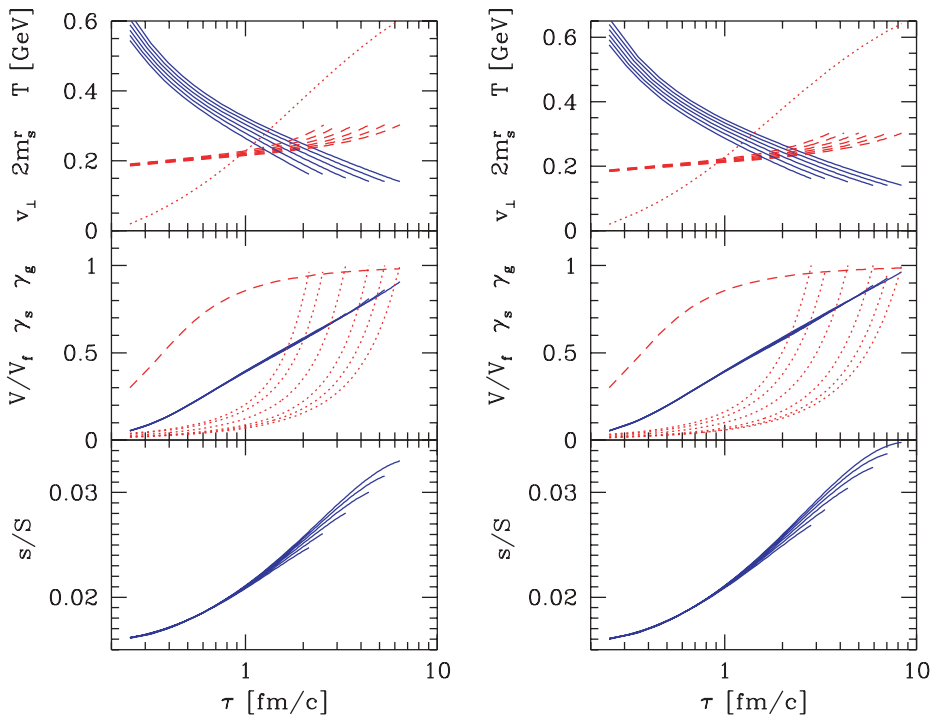

FIG. 3. (Color online) RHIC results. Top panel: solid lines show temperature T; dashed lines, running mass $m_s^r(T)$; dotted line, assumed profile of transverse expansion velocity $v_\perp(\tau)$. Different lines correspond to different centralities. Middle panel: solid line(s) γ_s, which nearly coincide for different centralities; dashed, the assumed $\gamma_g(\tau)$; dotted, the profile of the assumed volume, $[dV(\tau)/dy]/[dV(\tau_f)/dy]$ normalized by the freeze-out value. $R_\perp(\tau_0)$ stepped down for each line by factor 1.5. The end points, at maximum τ, allow us to identify corresponding s/S for different centrality in the bottom panel. Right and left: comparison of the two transverse expansion models, see Eqs. (19) and (20): left, bulk expansion (model V1); right, donut expansion (model V2).

entropy production is indeed increased by a factor of 4. From the perspective of strangeness production, this is one of the more interesting changes when comparing RHIC to LHC.

Given the volume as a function of τ and the associated conserved entropy content, we can evaluate the prevailing temperature T for any given quark and gluon chemical yield condition $\gamma_{q,s,g}$. The solid lines in the top panels of Figs. 3–7 show this result; in Figs. 3 and 4, they are on left for the V1 model and on right for the V2 (donut) model. The assumed γ_g is presented as a dashed line. In some of the top panels, we also show by the dotted line the time dependence of the applied transverse velocity, $v_\perp$, see Eq. (22).

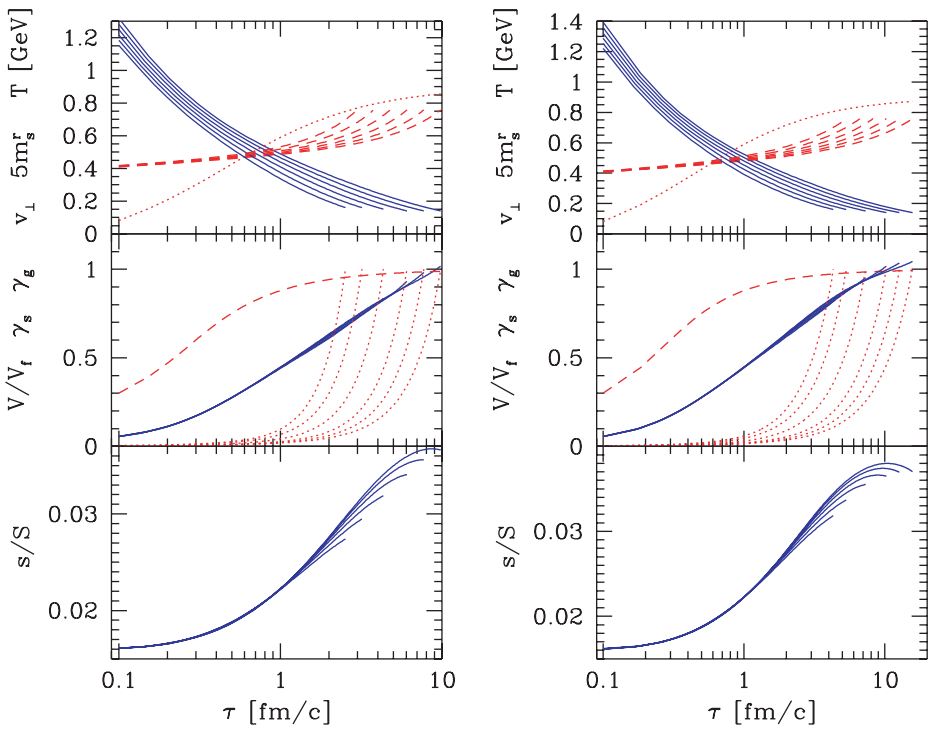

FIG. 4. (Color online) Same as Fig. 3, but for the LHC case. See text for discussion of differences with RHIC.

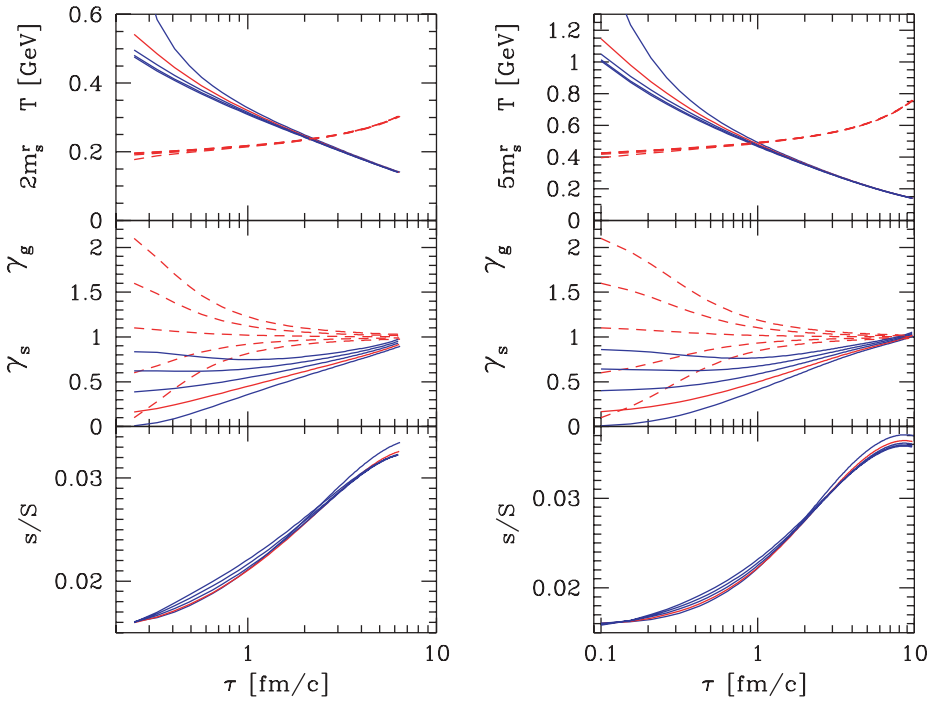

FIG. 5. (Color online) Model V1 (volume expansion) at RHIC (left) and LHC (right) for 5% most central collisions. s/S (bottom panel) and γ_s (solid lines, middle panel) as functions of τ, for widely varying initial gluon conditions (T in top panel; γ_g dashed, middle panel), constrained to same entropy content.

III. RESULTS ON STRANGENESS PRODUCTION

A. Benchmark results for RHIC

We present our results for strangeness production in QGP in Figs. 3–7. In Figs. 3 (RHIC) and 4 (LHC) we show the centrality dependence, with the two volume models, see Eqs. (19) and (20), corresponding to columns, with V1 on left and V2 (donut model) on right. In the following Figs. 5–7 we explore the dependence on the assumptions made. Here we show RHIC results on left and LHC results on right. In all Figs. 3–7 we show three panels above each other. As noted already, we show in the top panel, by solid line(s), the model time-temperature profiles. The experimental observables are shown as solid line(s) in the middle panel (γ_s) and in the bottom panel (s/S). The other lines illustrate as appropriate the key inputs used to obtain these results. When several lines of the same type are present, we are presenting the impact parameter dependence, scaling the size and entropy content as discussed above. In

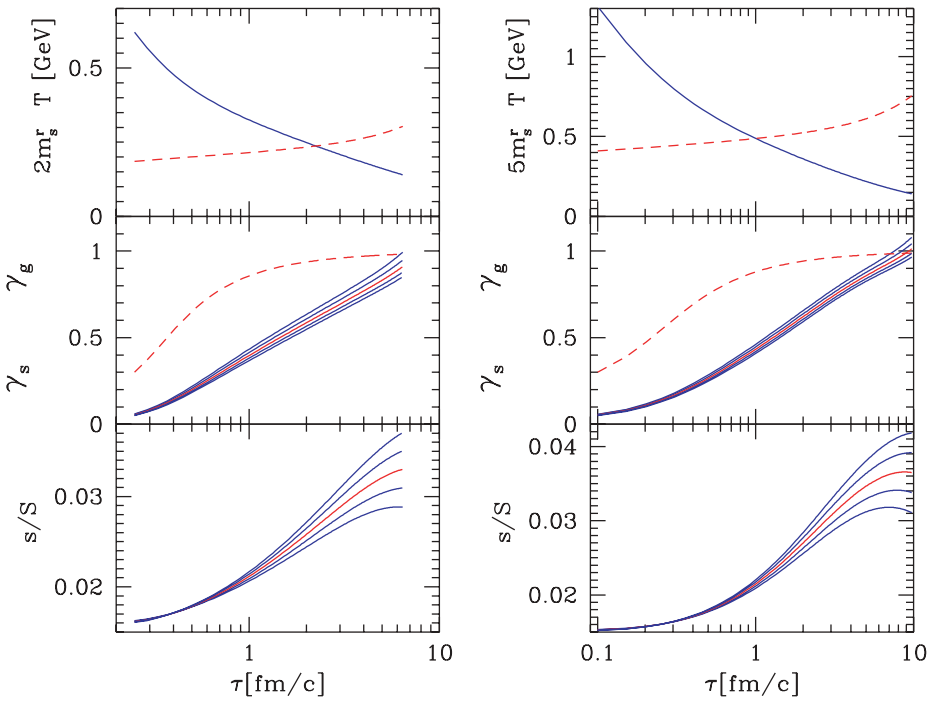

FIG. 6. (Color online) Study of of s/S evolution with τ for RHIC (left) and for LHC (right), V1 volume expansion model. Figure structure is same as Fig. 5. Middle panel, solid lines: computed evolution of γ_s in the deconfined phase for values of $k = 2, 1.5, 1, 0.5$, and 0, see Eq. (11). Bottom panel: corresponding evolution of s/S. Lowest γ_s line corresponds to $k = 0$ and the largest to $k = 2$, the opposite applies for s/S lines.

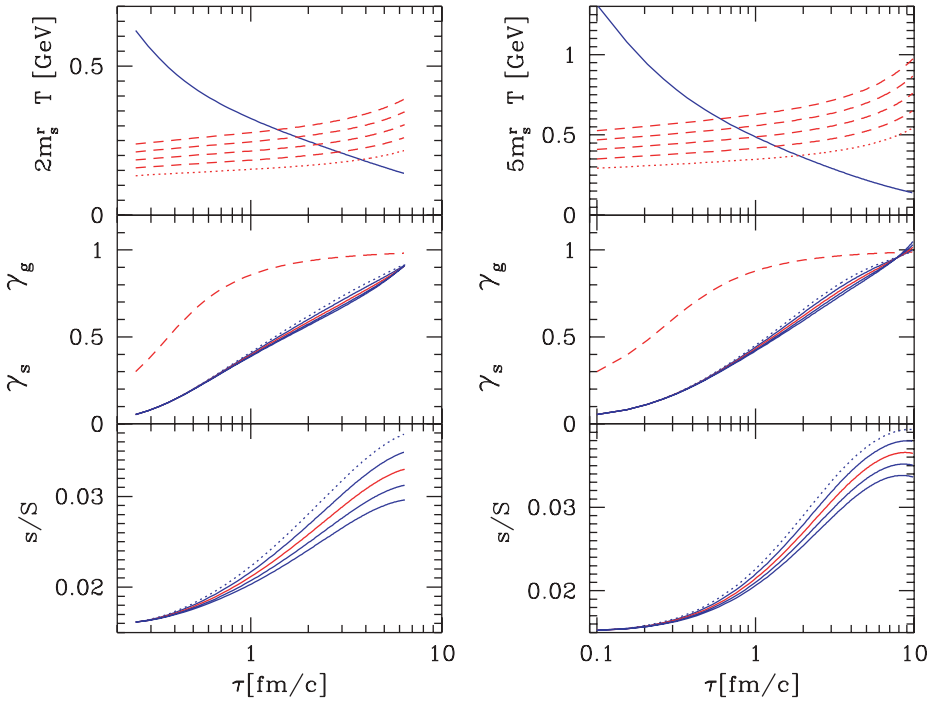

FIG. 7. (Color online) Study of s/S evolution with τ for different m_s, on left for RHIC, on right for LHC, V1 volume expansion model. Figure structure same as Fig. 5 and 6. Top panel: 5 (running) strange quark mass m_s^r. The middle of 5 lines being our standard reference value, see text for more detail.

general, the temperature is followed down to a freeze-out at $T_f = 0.14$ GeV.

In Fig. 3, we show what we believe is the best $\gamma_s(\tau)$ (solid lines, middle panel) and $s/S(\tau)$ (solid lines, bottom panel) for RHIC at 100 + 100 GeV at varying reaction centrality. The solid lines in the top panels show $T(\tau)$ for these six different centralities, with the lowest temperatures seen for the least central collisions; all temperatures continue to $T = 0.14$ GeV. The slight increase in the initial temperature with increasing centrality is the result of the scaling of initial entropy, which accommodates the observed change in $dS/dy|_f$ beyond participant scaling, see Eq. (23). For all centralities (and below also for RHIC), we assume the same initial $s/S(\tau_0) = 0.016$. All lines shown begin at $\tau_0 = 1/4$ fm, where the initial temperatures range $T_0 \in (0.55, 0.6)$ GeV. For the V1 model, the range of τ spans the interval $\tau_f = 2.2$ fm (most peripheral) to $\tau_f = 6.5$ fm (most central). In the donut expansion model V2, this range is $\tau_f = 3$–8 fm.

In the top panel, we also show the growth with τ of the transverse expansion velocity (dotted line), and the strangeness pair energy threshold $2m_s^r$ using running strange quark mass (dashed lines). We note that the temperature drops below this threshold for the most peripheral reactions considered already at $\tau = 1$ fm/c, and this occurs for the most central reactions at $\tau = 2$ fm/c, for model V1, and, respectively, 1.5 and 2.8 fm/c, for model V2. Thus, high-strength thermal strangeness production lifespan varies by as much as a factor of 3, depending on centrality and the expansion model.

In the middle panel, we show as a dashed line the rise of the gluon occupancy γ_g which we employed. The quark occupancy γ_q is following the same functional temporal evolution starting with a 2/3 smaller initial value and evolving 1.5 times slower. Because gluons dominate strangeness production in QGP, we do not show γ_q explicitly. The dotted lines show how the volume evolves toward its maximum value at freeze-out. Each line is normalized to unity at freeze-out. The actual value of the volume can be read off of Fig. 2, given the value of τ.

To summarize the key results: We see a gradual increase of strangeness yield with centrality, reaching near strangeness QGP equilibrium for the most central collisions at RHIC. We have checked stability of this result against variation of model assumptions. More detailed discussion will be presented further below, see, e.g., Fig. 6.

B. Strangeness production predictions for LHC

We performed a similar evaluation of strangeness production at LHC; see Fig. 4, which follows the same pattern as Fig. 3. Three modifications were introduced when we considered LHC:

(i) To account for the greater reaction energy, as already discussed, we increased the entropy dS/dy by factor 4, which implies an assumed increase in rapidity density of hadrons by a similar factor. We assumed that in elementary parton interactions, the relative strength of strangeness and nonstrange hadron production is unchanged, and thus we keep the initial relative yield $s/S = 0.016$ constant. Given the entropy yield increase, we implicitly assumed an increase in initial strangeness yield by a factor 4 at LHC compared to RHIC.

(ii) To accommodate the greater transverse expansion pressure, we increased the maximum transverse flow velocity which can now attain $v_\perp = 0.80\,c$ (dotted line, top panel Fig. 4).

(iii) We further assumed that thermalization time dropped from $\tau_0 = 1/4$ fm at RHIC to $\tau_0 = 1/10$ fm at LHC.

However, inspecting the slowly changing initial state evolution, in Fig. 4, there would be little change in our results if τ_0 were to remain unchanged between RHIC and LHC. At this early time, $\tau_0 = 1/10$, the value of $\gamma_s(\tau_0)$ at LHC is similar to the situation at RHIC; compare the beginning of the solid line in the middle panels of Figs. 3 and 4.

This is so, since the magnitude of the phase space scales with T^3 and the initial temperature $T(\tau_0)$ is considerably greater at LHC: in the top panel in Fig. 4, we see that it reaches up to $T = 1.25$ GeV. For this reason, we have to show in the top panel (dashed lines) $5m_s^r$ rather than $2m_s^r$, in order to fit it visibly into the top panel of the figure, and this is the only difference between the display of LHC results in Fig. 4 and that for the RHIC results in Fig. 3.

We note that despite a much greater expansion velocity, the evolution time at LHC is significantly longer, with the most central collisions taking up to 30% longer to reach the freeze-out temperature, $T_f = 0.14$ GeV. The reader who prefers earlier freeze-out, at, e.g., $T_f = 0.17$ GeV, can evaluate the changes required by consulting the temperature profiles shown in the top panel.

The different centralities at LHC are considered with the same scaling of the transverse size and entropy content as we did for the case of RHIC. Comparing the left-to-right set of results (i.e., volume V1 to donut V2 expansion models) for LHC, we see a more developed chemical equilibrium of strangeness with clear evidence of (over)saturation of yields for a few centralities, see the bottom right panel in Fig. 4. There is greater final specific strangeness content at LHC than at RHIC, with visibly greater thermal production leading to strangeness (over)saturation.

At RHIC, the thermal production raises the value of s/S from 0.016 to 0.028 for most central collisions (V1 model of bulk volume expansion), while at the LHC the thermal production raises s/S from 0.016 to 0.032. We will discuss below what this increase means for the K/π and other particle ratios. The same relative increase in s/S is seen in the model V2 of the expansion comparing RHIC and LHC. However, if the homogeneous bulk expansion applies at RHIC, but a donut type expansion arises at LHC, the increases in strangeness yield and lifespan would be more spectacular. Depending on its expansion dynamics, LHC clearly harbors the potential to surprise us.

C. Study of the dependence on initial thermalization condition

An important question is how the value of the unknown initial conditions impacts the results we presented above. We have studied this question in depth in many different model approaches. The answer "practically no dependence" is best illustrated in Fig. 5, which shows the more conservative volume expansion model V1 results for RHIC (left) and for LHC (right). We explore a wide range of initial gluon (and quark) occupancy γ_g, which for consistency with other figures is shown in the middle panel by dashed lines; the initial values we consider for glue occupancy vary as $0.1 < \gamma_g(\tau_0) < 2.1$ in step of 0.5. The second of these lines, from the bottom, is the reference behavior we used in Figs. 3 and 4.

We recall that with $\gamma_g(\tau_0)$, we also vary $\gamma_q(\tau_0)$, which follows the same functional temporal evolution starting with a 2/3 smaller initial value and evolving 1.5 times slower. Note also that the scale in the top panel varies between the RHIC (left) and LHC (right) cases, and the dashed lines denote $2m_s$ (left) and $5m_s$ (right). Since the initial values of $s/S = 0.016$ and $dS/dy = 5000$ on left for RHIC and $s/S = 0.016$ and $dS/dy = 20000$ on right for LHC are set, there is a corresponding variation in T_0 (top panel, left end of solid lines) and γ_s (left end of solid lines in middle panel). The final results for $\gamma_s(\tau_f)$ (right end of solid lines in middle panel) and $s(\tau_f)/S$ (bottom panel) are impressively insensitive to this rather exorbitant diversity of initial conditions at fixed entropy content. The spread in $s/S(\tau)$ we observe in the bottom panel could be seen as a wide line width.

We conclude that strangeness cannot probe the very initial QGP conditions near τ_0; the memory of the initial history of the reaction is lost, and the system is opaque for $\tau <$ 2–3 fm/c to the strangeness signature. On the other hand, and most importantly, for the present study, this also means that experimental observables are characteristic of the properties of nearly chemically equilibrated QGP.

However, there remains a dependence on the history of the QGP fireball in models in which gluon (and light quark) chemical equilibrium is not attained even in central reactions at RHIC [25,26]. Thus, only if gluons in QGP did not approach the chemical equilibrium at τ_f, a signature of this condition would be seen in the strangeness yield as is seen considering the right-hand side of Eq. (9). Correspondingly smaller values of s/S are then expected.

Yet, our results presented here agree well with current RHIC strange hadron production results regarding the total strangeness yield. This constitutes indirect evidence for the achievement of light quark and gluon chemical equilibrium in QGP formed in the most central, highest A and highest energy RHIC reactions. On the other hand, the relatively small size and short lifespan of a QGP potentially also formed in peripheral collisions could hinder the achievement of QGP chemical equilibrium at hadronization.

D. Fundamental uncertainties in strangeness production

There are two QCD-related uncertainties in our strangeness production study which we explore in turn in Figs. 6 and 7: (1) the effect of interaction on the number of strange quark degrees of freedom, Eq. (11), and (2) the value of strange quark mass. We will now show that these uncertainties lead to observable effects, particularly regarding the final value of s/S and, to a lesser extent, the final value of γ_s (chemical yield equilibration).

We first recall that γ_s is introduced in Eq. (2) in order to relate the prevailing strangeness density to the chemically equilibrated density at temperature T. Given a strangeness yield, the value of γ_s depends on the properties of QCD in terms of the chemically equilibrated density. The actual value of γ_s enters decisively into the kinetic equation of strangeness production. Equation (9) shows that the smaller the value of γ_s, the bigger is the change in the value of s/S.

Since in our approach we used Boltzmann statistics for the strangeness degree of freedom, the effect of Pauli blocking on strangeness production is not considered and in fact is a minor effect. The direct dependence of physical observables on γ_s arises from the process of strangeness reannihilation into gluons. We note that Eq. (9), describing the change in strange quark yield, can also be written in the form:

$$\frac{d}{d\tau}\frac{s}{S} = a_g\left(\rho_g^2\rho_s^{\infty 2} - \rho_s^2\rho_g^{\infty 2}\right) + a_q\left(\rho_q^2\rho_s^{\infty 2} - \rho_s^2\rho_q^{\infty 2}\right), \quad (24)$$

where instead of γ_i the actual densities of particles appear. We see that for each particle both the equilibrium and transient densities must enter in order for the system to attain chemical equilibrium as a function of time. Consequently, the value of γ_s and hence the QCD correction in Eq. (2) matters.

Figure 6, which follows the pattern of Fig. 5, illustrates this effect when the effective degeneracy, see Eq. (11), varies. We consider values of $k = 2, 1.5, 1., 0.5,$ and 0. $k = 2$ is the perturbative effect seen for massless quarks, and $k = 0$ corresponds to no effect of interaction, when $m_s \gg T$. When $k = 0$, the strange quark degeneracy is largest; thus for a given strangeness yield s, the value of γ_s is smallest and the production of strangeness biggest. Consequently, this value corresponds to the smallest γ_s in the middle panels of Fig. 6 and greatest value of s/S in the bottom panels. Other lines follow, and the middle solid lines (red online) correspond to $k = 1$, which we used to obtain the reference results presented earlier.

A similar effect arises considering variation of strange quark mass as shown by dashed lines in the top panels of Fig. 7. We vary by a factor of 2 the strange quark mass, as seen in the top panel of Fig. 7, for RHIC (left) and for LHC (right). When the strange quark mass is increased, the equilibrium strangeness density is decreased, and thus, for a given strangeness yield s/S, the value of γ_s is increased, which in turn reduces strangeness production strength. The smallest mass considered (dotted line in top panels of Fig. 7) corresponds to the largest final value of s/S (dotted line in the bottom panels). What is more surprising is that the effect of mass variation *cancels* in the actual computed γ_s shown in the middle panels. The reason for this accidental cancellation is that for a larger mass, the smaller value of final s/S solves for the same value of γ_s, see Eq. (10).

Since both m_s and the interaction effect on the strange quark effective degeneracy, see Eq. (11), are today not understood at a sufficiently precise level, the appearance of a possible range of values at freeze-out for both γ_s and s/S, in Figs. 6 and 7, signals (correlated) uncertainty in the understanding of the results at RHIC and predictive power for LHC.

IV. CONSEQUENCES FOR HADRON YIELDS AND THEIR EVOLUTION FROM RHIC TO LHC

A. Strangeness and entropy

The final value of s/S is the key result which practically alone determines the relative strange particle yields. It depends on the value of dS/dy that we start with. The value we take, $dS/dy = 20000$ at LHC (four times RHIC), is a guess arising from extrapolation of the energy dependence of particle production. However, it fixes in effect the initial conditions and leads to the range of values for s/S we obtained. We had found that there is continued growth of strangeness yield beyond the RHIC energy range where $dS/dy = 5000$, which suggests a further strong increase in the strange hadron yield we will address below.

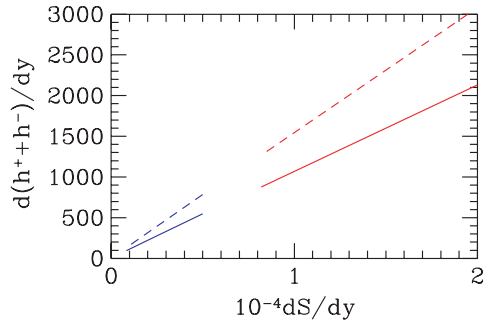

FIG. 8. (Color online) Yield of charged hadrons $d(h^- + h^+)/dy$ for different values of dS/dy, left domain for RHIC and right upper domain for LHC. Solid lines, before weak decays; dashed lines, after all weak decays.

Variation of dS/dy amounts to variation of the produced hadron yield. We expect that $dS/dy \propto dh/dy$. To quantify this, we present, in Fig. 8, how the yield of charged hadrons relates to the entropy yield. These results were obtained both for RHIC (left region, red online) and LHC (right region) by the methods described in Ref. [9], employing the SHARE suite of programs [40]. In this evaluation, we have available for each s/S (at RHIC and LHC) the corresponding strangeness occupancy γ_s. We further can fix the ratio of charge to baryon number as in the incoming nuclei, $q/b = 0.39$.

A further difference between RHIC and LHC is that we take the thermal energy per baryon at RHIC to be $E/b = 39.3$ GeV, whereas at LHC, $E/b = 412$ GeV (following Ref. [9]). The consistent ranges for s/S at RHIC are $0.018 < s/S < 0.03$; at LHC, we can address $0.018 < s/S < 0.037$, we cannot otherwise find a smooth match of QGP to HG phase space within the physical range of phase space occupancies γ_s, γ_q. We note that this LHC choice, $E/b = 412$ GeV, limits the range of possible entropy yield to just below the range we explore in our present work, $dS/dy = 20,000$, four times the RHIC range.

We next explore the resulting final s/S and γ_s. We show these quantities in Fig. 9 as functions of the dS/dy input (keft) and of the charged hadron multiplicity $d(h^- + h^+)/dy$ (right). The two expansion models we consider are, as before, V1 homogeneous expansion (thin solid, lower line) and V2 donut expansion model (thick solid, upper line). We see a gradual rise of both s/S and γ_s as function of dS/dy which begins to saturate for $dS/dy > 20000$, but at rather high values beyond chemical equilibrium: the expansion is so fast that there is no time to reannihilate the very abundant strangeness before freeze-out.

In Fig. 9 on the right-hand side, we see (smaller dh/dy range) the RHIC and LHC domains. Dashed lines are the charged hadron multiplicity after weak decays, in particular

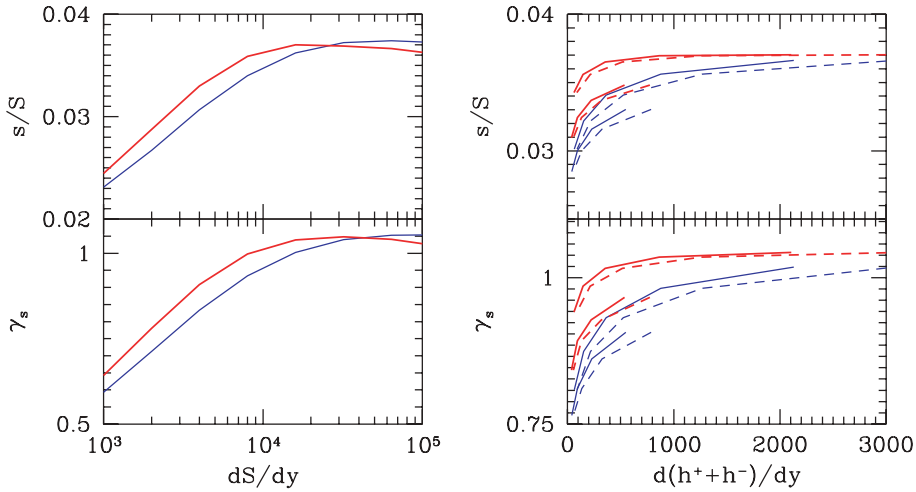

FIG. 9. (Color online) s/S (top panel) and γ_s (bottom panel) for the most central 5% collisions as function of dS/dy (on left) and as function of $d(h^+ + h^-)/dy$ on right. The bulk transverse expansion model V1 is the thin solid line (blue), the thick line (red) is the donut expansion model V2 with $d = 3.5$ fm. On right, solid lines: before weak decays, dashed lines: after weak decays (excluding $K^\pm$ see text). We recognize the RHIC domain results by the smaller dh/dy range of results presented.

of neutral strange hadrons such as K_S. The negligible impact of charged kaon weak decays to hadron multiplicity is not accounted for as this effect is small and experiment dependent considering the quasistability of $K^\pm$. In the RHIC domain, we have a nearly linear rise of s/S (top panel) and γ_s (bottom panel) with $d(h^+ + h^-)/dy$. In the LHC domain, chemical (over) saturation of these quantities is clearly visible. The left- and right-hand sides of Fig. 9 have at large dS/dy and $d(h^+ + h^-)/dy$, respectively, a similar appearance indicating chemical (over)saturation with the increasing hadron yield. We recall that while the functional form of the figure is correct, the normalization of the abscissa is somewhat arbitrary for the case of LHC, which is based on an extrapolation of SPS and RHIC results.

We next study the growth of strange hadron yield with s/S. In order to not confuse this with the issue of final hadronization volume of QGP, we will study particle ratios. The method of evaluating particle yields is the same as just discussed in the study of the charged hadron yield: the SHARE program is asked to match microcanonical conditions in the QGP phase to those of HG phase space. Given the statistical parameters, we can compute all particle yields within the statistical hadronization approach.

We first consider, in the two top panels of Fig. 10, the ratios Λ/π^+ and K^+/π^+ as functions of s/S, the attained specific strangeness per entropy at QGP freeze-out. Solid lines are before weak decays, and dashed lines present the corresponding results after weak decays. These enhance the pion yield, but as we see, even more the Λ yield. The K^+ yield is practically not changed: considering the long lifespan of the charged kaon, it is common to present experimental results corrected for any decay. Thus, $K^\pm$ are considered, in our study, as if they were stable particles. The RHIC results are the thicker lines and the LHC results are the thinner lines.

The RHIC and LHC results for $K^+/\pi^+, \phi/K^+$ and Ω^-/K^+ are practically overlapping, since the influence of the difference in baryochemical potential is not material for this ratio. However, the greater final s/S yield expected in most central LHC collisions implies an increased yield at LHC compared to RHIC. The dotted lines in the second panel from the top in Fig. 10 guide the eyes both in the RHIC domain and at the higher s/S, LHC domain.

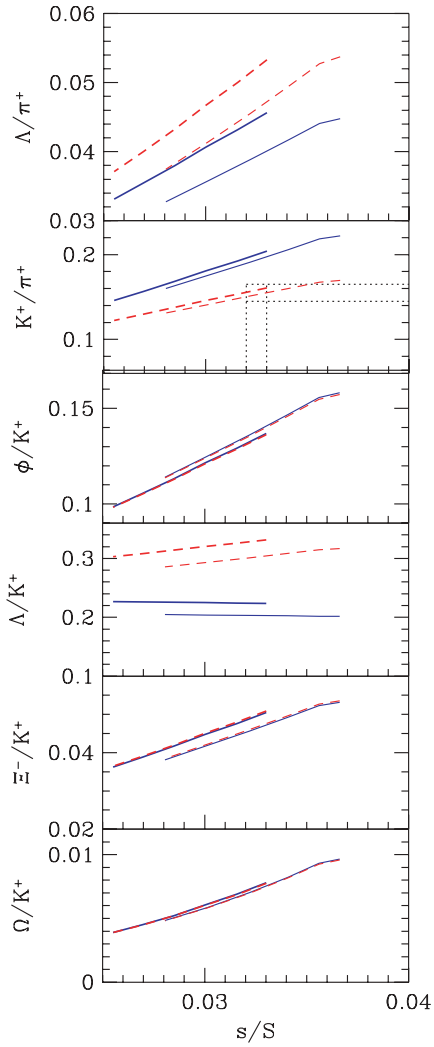

FIG. 10. (Color online) Relative particle yields as functions of s/S: from top to bottom $\Lambda/\pi^+, K^+/\pi^+$, followed by $\phi/K^+, \Lambda/K^+, \Xi^-/K^+$, and Ω^-/K^+. Solid lines (blue) are the primary relative yields, dashed lines (red) give the yields after weak decays (K^+ is not decayed). Thick line with $s/S < 0.03$ are for RHIC, and thin lines with $s/S < 0.037$ are for LHC physics environment. Dotted lines guide the eye for the RHIC K^+/π^+ ratio.

We find, in this perhaps easiest to measure K^+/π^+ ratio, a noticeable and measurable relative yield increase. This prediction is important, since after dropping with energy at SPS, this ratio remained of the same constant magnitude (within error) at the much higher RHIC energy domain. There is less change expected between RHIC and LHC for the Λ/π^+ ratio, since the decreasing baryochemical potential is compensating, to a large extend, the effect of the increase in strangeness yield. We note that there will be the opposite effect in the $\overline{\Lambda}/\pi^+$ yield. We see that the ratios ϕ/K^+ and Ω/K^+ are most sensitive to the change in s/S occurring between RHIC and LHC. The change in baryochemical potential diminishes this sensitivity considerably in the Ξ/K^+ ratio. Except for Λ/K^+, the weak decays have a negligible impact on all ratios with K^+ considered here.

B. Strange particle yields as function of centrality

We have obtained the growth of strangeness yield in QGP with centrality, and this allows us to explore participant dependence of strange hadron yields. Since we do not know well how E/b and E/TS change as centrality changes, we choose to follow a different approach in order to present our results. We assume that the hadronization occurs at a fixed condition, and first we consider $T = 140$ MeV and $\gamma_q = 1.6$, corresponding to supercooled sudden hadronization. In a second step, we compare these results with those obtained with $T = 160$ MeV and $\gamma_q = 1$, which is the equilibrium hadron phase space. The fixed value of statistical hadronization parameters as a function of centrality follows the pattern seen in the analysis of RHIC results [7].

To obtain the results, we follow a similar computational scheme as developed in the study of s/S dependence, except that we now fix T MeV and γ_q, and not, e.g., E/TS. These conditions lead to similar hadronization conditions, but E/TS had some variability for small participant number, see Fig. 4 in Ref. [7].

In Fig. 11, we show the results for RHIC (left) and LHC (right). We follow a similar display scheme as in Fig. 10, and show Λ/π^+, K^+/π^+, followed by ϕ/K^+, Λ/K^+, Ξ^-/K^+, Ω^-/K^+, as functions of participant number. The thinner (blue) lines are for the V1 model of volume expansion, and the thicker (red) lines for the V2 model

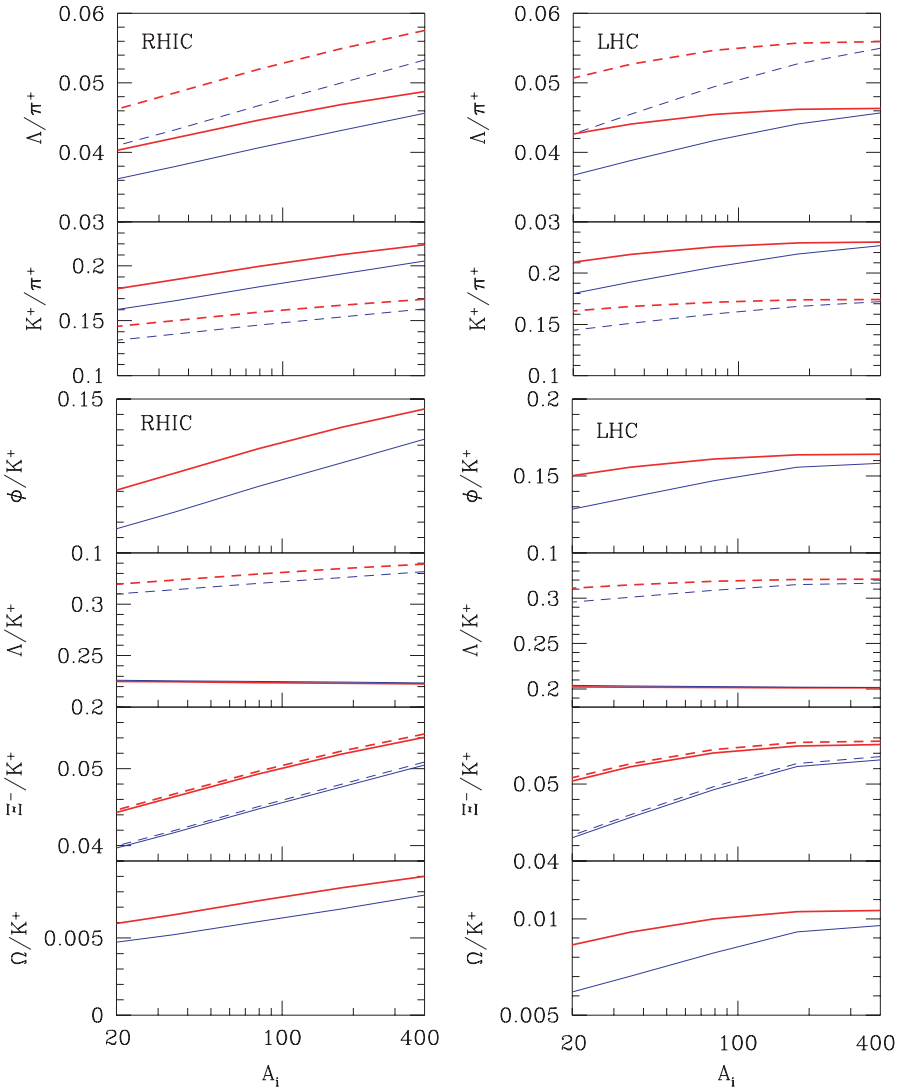

FIG. 11. (Color online) Relative strange particle yields as functions of participant number A, left RHIC and right LHC. From top to bottom: Λ/π^+, K^+/π^+, ϕ/K^+, Λ/K^+, Ξ^-/K^+, and Ω^-/K^+. Solid lines, primary relative yields; dashed lines, (relative) yields after all weak decays (not shown when difference is within line width). Thin lines (blue), model V1 (volume expansion); thick lines (red), model V2 (donut expansion). Results are for supercooled sudden hadronization.

of donut expansion. Dashed lines include the weak decays, which increase the Λ/π^+ ratio and decrease the K^+/π^+ ratio.

We see, in Fig. 11, a steady, but rather slow, increase with centrality of the relative strange hadron, to nonstrange pion yield. The decay pions tend to flatten the K^+/π^+ ratio at RHIC. We predict more rise of ϕ/K^+ than is observed at RHIC [41], but our variation is within the error bar of the experimental, nearly constant result, $\phi/K^+ = 0.15 \pm 0.03$. As discussed earlier, the overall increase in s/S expected at LHC (right) compared with RHIC (left) explains the noticeably greater relative K^+/π^+ ratios at LHC. The most noticeable rise, with centrality, is expected when the ratio has the largest disparity in strangeness content. There is no centrality dependence expected when there is no difference in strangeness content, such as in Λ/K^+, where the weak decay produces very small centrality dependence.

One of the interesting questions is how sensitive is the study of these particle ratios to the hadronization conditions. In Fig. 12, we compare the sudden hadronization at $T = 140$ MeV and $\gamma_q = 1.6$ with the hadron phase space equilibrium model at $T = 160$ MeV and $\gamma_q = 1$ forming the ratio of particle yield ratios, that is, the results obtained for sudden hadronization are divided by those obtained for the equilibrium HG phase space. The panels follow the same particle ratios as in Fig. 11, with RHIC (left) and LHC (right) results.

The value of $\gamma_s^H(T = 160, \gamma_q^H = 1)$ varies as a function of centrality $1.26 < \gamma_s^H < 0.88$. In general, the higher hadronization temperature assumed in this chemical equilibrium case favors the yield of the more massive hadron. Thus, ratios of heavy to lighter particles evaluated at the same value of s/S as shown in Fig. 11 are bigger for the $\gamma_q^H = 1$ since we took a higher $T = 160$ MeV chemical equilibrium freeze-out value.

We note that the nonequilibrium model is much better for explaining available multistrange hadron data. The equilibrium model needs to be amended to explain the enhanced Ω yield. The way out from this dilemma if one insists on HG equilibrium could be a multifreeze-out temperature interpretation. The freeze-out temperature of the Ω^- in the equilibrium freeze-out model would need to be noticeably higher than that of the bulk of strange particles. We note that such multifreeze-out models could experience systematic difficulties as a function of centrality. Moreover, considering Fig. 12, in the chemical equilibrium interpretation of hadron production, a separate freeze-out for both Ω^- and Ξ^- would be required at LHC. Aside from being unpalatable, such a

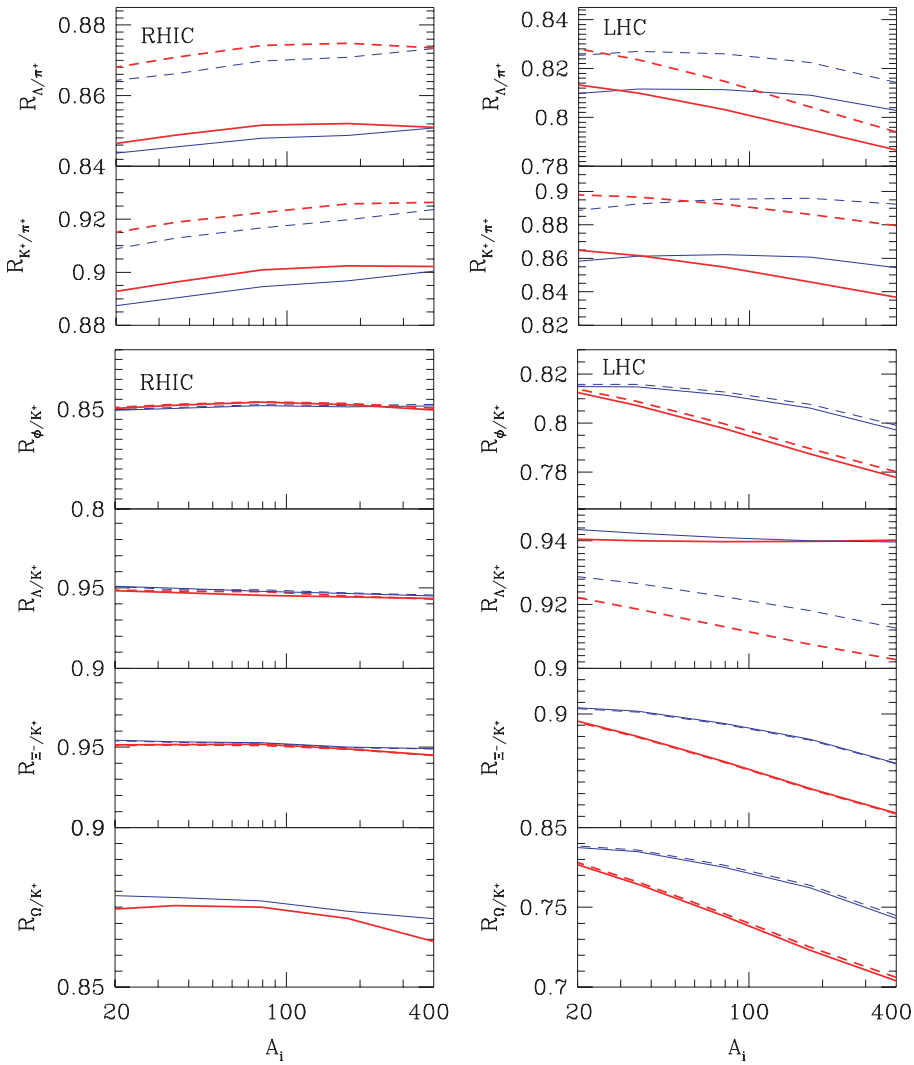

FIG. 12. (Color online) Ratio of relative yields obtained for sudden and equilibrium hadronization (see text) as function of centrality. Left RHIC, and right LHC. Same particle ratios as in Fig. 11. Solid lines, primary relative yields; dashed lines, (relative) yields after all weak decays (when absent, no difference within line width with solid lines). Thin lines (blue), model V1 (volume expansion); thick lines (red), model V2 (donut expansion).

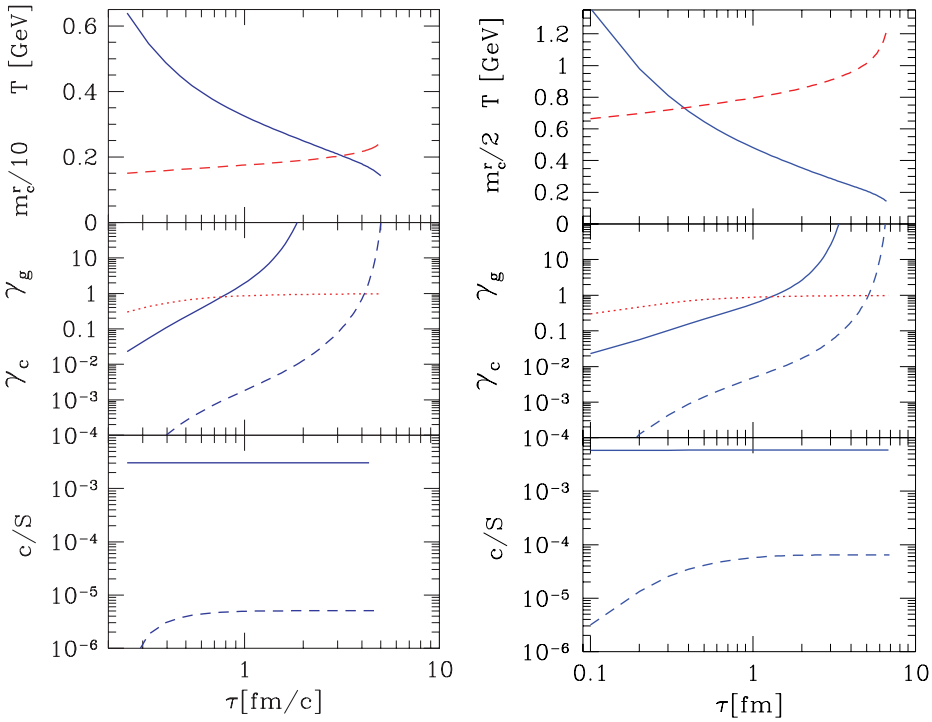

FIG. 13. (Color online) Left RHIC and right LHC for charm production. Figure structure same as Figs. 3–7. Top panel: solid lines, T; dashed lines, running m_c^r, scaled with 10 for RHIC on left, and with 2 on right for LHC. Middle panel: dotted line, γ_g; solid lines the computed total charm, γ_c; dashed lines, γ_c corresponding to thermal charm production. Bottom panel: specific charm yield per entropy, solid lines for all charm, and dashed lines for thermally produced charm.

multifreeze-out HG equilibrium model would not describe fluctuations well [29].

C. Thermal charm at RHIC and LHC

The direct initial high energy parton collisions dominate production of the massive flavor, charm and bottom, and a thermal process seems to be of no interest. However, there are two questions we can investigate:

(i) Considering that γ_c in the deconfined phase can be as large as $\gamma_c \simeq 100$, is there any significant thermal annihilation of charm in the QGP evolution?
(ii) How large is the thermally produced charm yield and can it lead to chemical equilibrium of charmed quarks?

The interest in question (a) needs no further discussion. Question (b) is of interest because the directly produced charmed quarks are in principle not easily thermalized, while the thermally produced charmed quarks emerge naturally in a momentum distribution, imaging the thermal momentum distribution of their parent particles. Consequently, the thermally produced charmed quarks provide a solid thermal lower limit for the yield of charm, with the directly produced charm contributing to thermal distribution after charm has been subject to collisions required for thermalization.

We see the results of this study in Fig. 13 for RHIC and LHC. The top panels, as usual, present the temperature and charmed quark mass, scaled with factor 1/10 at RHIC and 1/2 at LHC. The middle panel presents γ_g, the charm phase space occupancy γ_c, and γ_c obtained solely by *thermal processes*. Similarly, the bottom panels show the thermal yield at RHIC and LHC, and the (little) evolving c/S yields, including the directly produced charm. The direct charm production, at RHIC, is expected to be 600 times greater than the thermal process. At LHC, the higher initial temperature, but unchanged specific direct yield c/S, in parton collisions, suggests that thermal production is just 90 times smaller. However, this factor depends on a good understanding of both processes and the initial conditions and surely cannot be fully trusted. Moreover, there is the possibility that the directly produced charm at LHC may not be well thermalized, in which case an appreciable fraction of thermal charm yield could indeed originate in thermal reactions.

The answers to the opening questions, thus, are

(i) There is no visible charm reannihilation, see the nearly horizontal lines at $c/S = 3 \times 10^{-3}$ (left, RHIC) and $c/S = 6 \times 10^{-3}$ (right, LHC), in the bottom panel; note that the direct charm yield, we assumed implicitly, is obtained by multiplying the c/S yields with $dS/dy = 5,000$ on left for RHIC, yielding $dc/dy|_{\rm RHIC} = 15$, and with $dS/dy = 20,000$ on right for LHC, yielding $dc/dy|_{\rm LHC} = 120$.
(ii) In the middle panel, we see that thermal production alone (dashed lines) oversaturates the charm phase space; the thermally produced charm phase space occupancy $\gamma_c^{\rm th}$ (dashed lines, middle panels) crosses the gluon dotted γ_g line at around 4 fm/c for RHIC (corresponding to $T \simeq 0.175$ GeV) and at 5 fm/c ($T \simeq 0.20$ GeV) at LHC.

V. SUMMARY AND CONCLUSIONS

We have studied the thermal QGP-based strangeness production at RHIC and LHC and interpreted the observed final s yield in terms of our theoretical knowledge about the properties of the QGP phase. Our aim has been to understand how the overall final state strange quark flavor has been produced, and to study in detail the mechanisms behind strangeness enhancement. As a further objective, we have explored the impact of high strangeness on the strange hadron yields.

Our results suggest that strangeness enhancement could be studied considering

$$R^s_{\rm CP} \equiv \frac{s/S|_{\rm central}}{s/S|_{\rm peripheral}} = \frac{s/S(\tau_f)}{s/S(\tau_0)}. \qquad (25)$$

The central strangeness yield is just the final value we find at freeze-out, combining the initial yield with the additional thermal production. The peripheral yield is the initial value before thermal strangeness production begins. Our study shows that $R^s_{\rm CP} \in [1.6, 2.2]$, with the precise result depending on details such as strange quark mass, see Fig. 7, reaction energy, and dynamics of expansion, see Fig. 2.

More generally, to separately consider s and S we can use $d(h^+ + h^-)/dy$ as a measure of entropy dS/dy content, see Fig. 8. Instead of the total strangeness, one may consider enhancement of individual (multi)strange particles, which we discussed in depth both as a function of the achieved s/S, in Sec. IV A, and as a function of centrality A at fixed hadronization condition for all centralities, in Sec. IV B.

We note that the overall growth of the enhancement of the strangeness yield with centrality, at the level a factor of 1.6–2.2, is accompanied by a further enhancement of multistrange hadron yields, as is seen when comparing the yields of multistrange hadrons with the yield of kaons. One can show that the ϕ/K^+ ratio is mainly dependent on the value of s/S and not on hadronization temperature (see Appendix B2i of Ref. [42]) when the strangeness conservation constraint is implemented. This effect is unique to ϕ and arises since $m_\phi \simeq 2m_K$.

Aside from centrality dependence, we have explored, within the framework of our model, the extrapolation from RHIC to LHC physics environments. More generally, we have presented, in Fig. 9, the reaction energy dependence by considering the central rapidity s/S yields as a function of dS/dy.

One of the interesting results obtained is the approach to chemical strangeness equilibrium in the deconfined QGP phase formed in most central and high energetic RHIC reactions. The evidence for this is implicit in the experimentally reported yields of strange hadrons, which lead to values of specific strangeness per entropy at the level of $s/S \simeq 0.03$ [7]. Our study of QGP-based kinetic strangeness production provides an explanation of this result, both in terms of the value of s/S and as a function of centrality.

Our present study further shows that the proximity of chemical strangeness yield equilibration in QGP formed at RHIC and LHC, and the effective opacity of QGP to this signature, is the reason that considerably less sophisticated models of QGP evolution which we, and others, have considered are equally successful in the study of the strangeness production, as long as these models yield conditions near to the chemically equilibrated QGP.

Given the near chemical equilibration at RHIC, and within the models considered, we obtain some strangeness over saturation at LHC. Moreover, for the most central 5% reactions there is no relevant dependence of strangeness production on initial conditions prevailing in the reaction. We have demonstrated this in a picture-book fashion, see Fig. 5, where, for a wide range of initial conditions, the same final strangeness yield and equilibrium condition arises after $\Delta\tau$ =2–3 fm/c evolution.

On the other hand, the more peripheral reactions do not saturate the phase space, in that both $\gamma_s^{\rm QGP} < 1$, and $s/S < 0.03$. Thus, the peripheral yields, being sensitive to the initial conditions, allow exploration of physical conditions in the QGP prior to the onset of chemical reactions. Therefore, our results for most peripheral reactions are also somewhat dependent on model assumptions about initial state and evolution dynamics.

We have shown, in Figs. 3 and 4, the impact parameter dependence that arises in two volume expansion models. Since the analysis results presented in Ref. [7] were used to fine tune the dynamical evolution model at RHIC, there is good qualitative agreement with experimental results. Our objective here has been to learn how to extrapolate the dynamics of strangeness production to the LHC environment. The gradual rise of strangeness yield s/S with dS/dy, seen in Fig. 9, is reminiscent of the rise of s/S with reaction energy obtained in an analysis of particle yields obtained at SPS and RHIC at different reaction energies [37].

We have made a (conservative) prediction regarding the increase in the K^+/π^+ ratio at LHC compared with that at RHIC, see Fig. 10. Though an important result is that we expect an increase at LHC, we note that even a greater increase is possible, signaling even greater values of s/S, depending on both (1) the dynamics of the volume expansion, which can enhance the strangeness oversaturation of the final QGP state, see Figs. 3 and 4, and (2) QCD details, such as strange quark density including QCD interactions, and (still not well understood) strange quark mass, see Figs. 6 and 7. In any case, we believe that this simple observable will show again strangeness production growing faster than entropy production; its increase is directly coupled to an increase in s/S. We note again that in our study the increase of s/S with centrality implies that ϕ/K^+ also increases with centrality.

A natural result is the finding of the chemical yield equilibration of strangeness in the QGP formed in the 5% most central top RHIC energy reactions. This leads to a better understanding of the resulting oversaturation of the hadron phase space by strangeness. The magnitude of this effect, dependent on the temperature of hadronization, can be considerable. This can be easily seen considering the magnitude of s/S in both QGP and HG phases. The final state hadrons formed far-off chemical equilibrium cannot significantly adjust chemical composition, considering the rapid breakup of the fireball, during the period of about 1–2 fm/c prior to onset of the free flow. Thus, our finding is

that strangeness-rich QGP enhances decisively the yields of multistrange hadrons. This phenomenon is more accentuated considering charmed hadrons containing strangeness, a topic under current investigation.

Furthermore, using the methods developed here, we have considered thermal charm production. At LHC, we find a nearly physically relevant thermal charm production, but not at RHIC. However, the thermal process we consider is able to produce enough charm to oversaturate the final state at both RHIC and LHC, see Fig. 13. This also shows that the direct parton collision based production at RHIC leads to extraordinarily large values of γ_c. The chemical nonequilibrium of charm is thus more pronounced than that of strangeness.

In conclusion, the totality of our results shows that as function of entropy yield dS/dy (equivalently, the reaction energy of $A_1 - A_2$ collision) and geometric reaction size (impact parameter dependence, participant number A), the phenomenon of strangeness enhancement is well described by the mechanism of QGP-based thermal gluon fusion strangeness production. We find both as functions of centrality and energy, a gradual increase in specific strangeness yield, which agrees with all available experimental results. We find that as a function of energy, this continues from RHIC to LHC, thus increasing our hopes for a more clear strangeness signature of deconfinement.

ACKNOWLEDGMENTS

Work was supported by the U.S. Department of Energy, Grant No. DE-FG02-04ER4131. Work at LPTHE, Univ. Paris 6 et 7 is: Unité mixte de Recherche du CNRS, UMR7589.

[1] B. B. Back *et al*., Nucl. Phys. **A757**, 28 (2005).
[2] J. Rafelski and B. Müller, Phys. Rev. Lett. **48**, 1066 (1982); **56**, 2334(E) (1986).
[3] J. Letessier, A. Tounsi, and J. Rafelski, Phys. Lett. **B389**, 586 (1996).
[4] J. Rafelski, J. Letessier, and A. Tounsi, Acta Phys. Pol. B **27**, 1037 (1996).
[5] P. Koch and J. Rafelski, Nucl. Phys. **A444**, 678 (1985).
[6] P. Koch, B. Muller, and J. Rafelski, Phys. Rep. **142**, 167 (1986).
[7] J. Rafelski, J. Letessier, and G. Torrieri, Phys. Rev. C **72**, 024905 (2005).
[8] J. Letessier and J. Rafelski, Phys. Rev. C **73**, 014902 (2006).
[9] J. Rafelski and J. Letessier, Eur. Phys. J. C **45**, 61 (2006).
[10] P. Koch, J. Rafelski, and W. Greiner, Phys. Lett. **B123**, 151 (1983).
[11] P. Braun-Munzinger, K. Redlich, and J. Stachel, in *Quark Gluon Plasma 3*, edited by R. C. Hwa and Xin-Nian Wang (World Scientific, Singapore, 2004).
[12] J. Rafelski and M. Danos, Phys. Lett. **B97**, 279 (1980); J. Rafelski and J. Letessier, J. Phys. G **28**, 1819 (2002).
[13] S. Hamieh, K. Redlich, and A. Tounsi, Phys. Lett. **B486**, 61 (2000).
[14] K. Redlich and A. Tounsi, Eur. Phys. J. C **24**, 589 (2002).
[15] J. Kapusta and A. Mekjian, Phys. Rev. D **33**, 1304 (1986).
[16] Jan-e Alam, B. Sinha, and S. Raha, Phys. Rev. Lett. **73**, 1895 (1994).
[17] K. Geiger, Phys. Rev. D **46**, 4965 (1992).
[18] L. Xiong and E. V. Shuryak, Phys. Rev. C **49**, 2203 (1994).
[19] Z. Xu and C. Greiner, Phys. Rev. C **71**, 064901 (2005).
[20] J. Rafelski and J. Letessier, Nucl. Phys. **A702**, 304 (2002).
[21] P. Koch, B. Muller, and J. Rafelski, Z. Phys. A **324**, 453 (1986).
[22] T. Matsui, B. Svetitsky, and L. D. McLerran, Phys. Rev. D **34**, 783 (1986); **37**, 844(E) (1988).
[23] T. S. Biro, E. van Doorn, B. Muller, M. H. Thoma, and X. N. Wang, Phys. Rev. C **48**, 1275 (1993).
[24] J. Rafelski and J. Letessier, Phys. Lett. **B469**, 12 (1999).
[25] D. Pal, A. Sen, M. G. Mustafa, and D. K. Srivastava, Phys. Rev. C **65**, 034901 (2002).
[26] Z. J. He, J. L. Long, Y. G. Ma, G. L. Ma, and B. Liu, Phys. Rev. C **69**, 034906 (2004).
[27] J. Letessier and J. Rafelski, J. Phys. G **25**, 295 (1999); J. Letessier and J. Rafelski, Phys. Rev. C **59**, 947 (1999).
[28] F. Becattini, M. Gazdzicki, A. Keranen, J. Manninen, and R. Stock, Phys. Rev. C **69**, 024905 (2004).
[29] G. Torrieri, S. Jeon, and J. Rafelski, Phys. Rev. C **74**, 024901 (2006).
[30] H. T. Elze, J. Rafelski, and L. Turko, Phys. Lett. **B506**, 123 (2001).
[31] T. Sjostrand, L. Lonnblad, S. Mrenna, and P. Skands, PYTHIA 6.3: Physics and Manual, arXiv:hep-ph/0308153, see in particular Sec. 12, p. 337ff.
[32] M. Bedjidian *et al*., Chapter 3 in CERN-Yellow Report 2004–2009, Proceedings of the CERN workshop "Hard Probes in Heavy Ion Collisions at the LHC," see http://cdsweb.cern.ch/search.py?recid=815037&ln=en, arXiv:hep-ph/0311048.
[33] S. Mrowczynski, Acta. Phys. Pol. B **37**, 427 (2006).
[34] J. Letessier and J. Rafelski, Phys. Rev. C **67**, 031902(R) (2003).
[35] J. Letessier, J. Rafelski, and A. Tounsi, Phys. Rev. C **50**, 406 (1994).
[36] T. S. Biro, P. Levai, and B. Muller, Phys. Rev. D **42** 3078 (1990).
[37] J. Letessier and J. Rafelski, arXiv:nucl-th/0504028.
[38] J. Letessier and J. Rafelski, *Hadrons and Quark-Gluon Plasma, Cambridge Monogr. Part. Phys. Nucl. Phys. Cosmol*., **18** Cambridge University, Cambridge, England (2002).
[39] S. A. Chin and A. K. Kerman, Phys. Rev. Lett. **43**, 1292 (1979).
[40] G. Torrieri, S. Steinke, W. Broniowski, W. Florkowski, J. Letessier, and J. Rafelski, Comput. Phys. Commun. **167**, 229 (2005) [arXiv:nucl-th/0404083]; G. Torrieri, S. Jeon, J. Letessier, and J. Rafelski, *ibid*. **175**, 635 (2006).
[41] J. Adams *et al*. (STAR Collaboration), Phys. Lett. **B612**, 181 (2005).
[42] I. Kuznetsova and J. Rafelski, arXiv:hep-ph/0607203.